Journal of Materials Chemistry B

RSC Publishing

PAPER

View Article Online
View Journal | View Issue

Cite this: J. Mater. Chem. B, 2013, 1, 2415

Fabrication, characterization and sensor application of electrospun polyurethane nanofibers filled with carbon nanotubes and silver nanoparticles

Zhaofei Ouyang,†[a] Jingfeng Li,†[ab] Jinhui Wang,[a] Qian Li,[a] Tongyang Ni,[a] Xiaoyuan Zhang,[a] Haixia Wang,[a] Qing Li,[b] Zhiqiang Su*[a] and Gang Wei*[b]

We reported here the electrospinning preparation of polyurethane nanofibers filled with carbon nanotubes and silver nanoparticles (PU–MWCNT–AgNP) and the subsequent fabrication of a novel non-enzymatic amperometric biosensor for analytical determination of hydrogen peroxide. The morphologies of the as-spun PU–MWCNT–AgNP hybrid nanofibers were observed by scanning and transmission electron microscopy. The interaction between MWCNTs and AgNPs in the electrospun nanofibers was studied by differential scanning calorimetry and dynamic mechanical analysis. The cyclic voltammetry experiments indicate that PU–MWCNT–AgNP nanofiber modified electrodes have high electrocatalytic activity on hydrogen peroxide, and the chronoamperometry measurements illustrate that this electrospun sensor has high sensitivity for detecting hydrogen peroxide. Our study further confirms the remarkable synergistic effect of MWCNTs and AgNPs on the significant improvement of the conductivity of electrospun nanofibers and the electrocatalytic activity, as well as the sensitivity of the fabricated non-enzymatic sensor. Under an optimal experimental condition, the created biosensor for detecting hydrogen peroxide has a sensitivity of 160.6 μA mM^{-1} cm^{-2}, a wide linear range from 0.5 to 30 mM and a detection limit of 18.6 μM ($S/N = 3$), which indicates that this novel and simple strategy for fabricating electrochemical sensor by an electrospinning technique has wide potential applications in bio-analysis and detection.

Received 28th January 2013
Accepted 12th March 2013

DOI: 10.1039/c3tb20316f

www.rsc.org/MaterialsB

1 Introduction

In recent years, the analytical determination of hydrogen peroxide (H_2O_2) has attracted growing attention, ascribable to both the fact that it is the end product of many enzymatic reactions and that it is essential in food, pharmaceutical, clinical and environmental analysis.[1–4] Many techniques, such as spectrophotometry,[5] chemiluminescence,[6] and electrochemistry,[7,8] have been employed for the determination of H_2O_2 previously. Among these methods, electrochemical detection has become the research focus due to its simplicity and low cost. Particularly, the non-enzymatic electrochemical sensor has attracted more interest compared to the enzyme-based sensors due to its simplicity, high stability and good reproducibility.[9,10]

It has been reported that metal nanoparticles (MNPs), such as Ag, Au, and Pt, exhibit good electrocatalytic activity toward H_2O_2.[11–15] For instance, Guascito *et al.* reported an amperometric sensor prepared by drop-casting AgNPs capped in a PVA colloidal suspension onto a Pt electrode, and found that AgNPs were able to improve electrocatalytic properties of the created sensor.[15] Meanwhile, carbon nanotubes (CNTs) have been widely used as an ideal catalyst supporting material since its discovery,[16,17] due to their large surface-to-volume ratio and the ability to promote electron transfer reactions. Therefore, to further improve the performance of the electrochemical H_2O_2 sensor, CNTs were also employed to modify the electrodes. In the past years, CNT–MNP nanohybrids have been synthesized and used for the fabrication of H_2O_2 sensors.[18–21] To prepare the CNT–MNP nanohybrids, electrochemical, chemical and physical methods have been employed.[4,22–25] However, most of these methods are verbose and complex, requiring different kinds of chemicals, irradiations and templates.[4,23] For example, in the study of Wu *et al.*,[24] gamma-ray irradiation was employed to functionalize multi-walled CNTs (MWCNTs), and MWCNT–polymer–Ag hybrids were synthesized relying on covalently bonded polymers. Wei *et al.* immobilized hemoglobin (HGB) onto the surface of MWCNTs and used the prepared MWCNT–HGB as a bio-inspired template to mediate the formation of Pt NPs, creating MWCNT–PtNP nanohybrids.[25] Therefore, it is desirable to develop a simple, mild and effective strategy to prepare well dispersed CNT–MNP nanohybrids.

[a]State Key Laboratory of Chemical Resource Engineering, Beijing University of Chemical Technology, 100029 Beijing, China. E-mail: suzq@mail.buct.edu.cn
[b]Hybrid Materials Interface Group, Faculty of Production Engineering, University of Bremen, D-28359 Bremen, Germany. E-mail: wei@uni-bremen.de; Fax: +49 421 218 64599

† These authors contributed to the work equally.

Electrospinning is known as a simple process technique to synthesize multifunctional, hierarchically organized polymer-functional material hybrid nanofibers with exceptionally long length, uniform diameter and large surface area.[26] It has been widely used in the preparation of enzyme-based electrochemical sensors.[27–30] However, relatively few examples of non-enzymatic electrochemical sensors based on electrospun nanofiber modified electrodes have been reported.[31,32] For example, Liu *et al.* reported an electrochemical sensor by casting carbon nanofibers (CNFs) suspension onto the surface of a carbon paste electrode (CPE).[31] The CNFs were prepared through calcinations of electrospun polyacrylonitrile (PAN) nanofibers. More recently, in the report of Wang *et al.*[33] hollow CuO particles have been prepared by the combination of electrospinning and thermal treatment processes, and then fabricated a H_2O_2 sensor by dropping CuO particles–Nafion–water suspension onto the surface of a well-polished CPE. Obviously, both of the thermal treatment processes and the traditional casting method were employed in their work,[31–33] which, however, could result in some drawbacks. Although the hybrid nanofibers would be more conductive by calcinations, the MNPs might agglomerate, and the fibrous morphologies of hybrid nanofibers could be destroyed through the elevated temperature treatment processes, which would negatively affect the electrochemical properties of the sensors.

Herein, we propose a new and facile method to create combinations of CNTs and MNPs by electrospinning, and fabricate a H_2O_2 non-enzymatic biosensor by directly electrospinning the polymer–CNT–MNP nanofibers onto the surface of a glassy carbon electrode (GCE). This strategy has many obvious advantages. It is very simple and fast without the use of thermal treatment processes and traditional casting methods, as well as the complex processes to fabricate well dispersed CNT–MNP nanohybrids; and no enzyme is used. In our work, considering the high electrocatalytic activity towards H_2O_2 and the low cost,[34] AgNPs were selected as the redox mediators. PU was employed as the polymer matrix due to its good spinnability and mechanical properties.[35,36] By simply blending the suspension of modified MWCNTs and commercialized AgNPs with the PU electrospinning solutions and then electrospinning, PU–MWCNT–AgNP hybrid nanofibers were successfully prepared. We found that the AgNPs were successfully adsorbed onto the surface of MWCNTs, and the MWCNTs were well dispersed and aligned in the nanofibers. The interaction between MWCNTs and AgNPs in the electrospun nanofibers was thoroughly investigated through differential scanning calorimetry (DSC) and dynamic mechanical analysis (DMA) tests. Their synergistic effect was also explored by testing the electrical conductivity of the hybrid nanofibers. Based on the advantages of MCNTs and AgNPs for detection of H_2O_2, the created PU–MWCNT–AgNP hybrid nanofibers were then directly electrospun onto the surface of a GCE to fabricate a non-enzymatic amperometric biosensor for highly sensitive detection of H_2O_2.

The electrochemical results not only confirm the remarkable synergistic amplification effect of MWCNTs and AgNPs in the electrospun nanofibers on H_2O_2 detection, but also reveal the superiority of our electrospinning method over the traditional casting method in preparation of electrochemical sensors. By electrospinning, MWCNTs can be well dispersed and aligned in the nanofibers, which can facilitate both the electron transfer and the uniform dispersion of AgNPs along the nanofibers. In addition, the electrospun nanofibrous membranes are highly porous, which are beneficial to the adsorption of electrolytes and the diffusion of reactants. Both features can help to improve the electrocatalytic activity of electrodes.

2 Experimental section

2.1 Reagents and materials

MWCNTs (>98% purity, 10–20 nm in diameter and ~15 μm in length), AgNPs (particle size < 100 nm, 99.5% trace metals basis) and Nafion solution (~5% in a mixture of lower aliphatic alcohols and water) were purchased from Sigma-Aldrich. Hexafluoroisopropanol (HFIP, >99.5% purity) was obtained from Lianyungang Tetrafluor New Materials Co., Ltd. (Jiangsu, China). Disodium hydrogen phosphate (Na_2HPO_4), sodium dihydrogen phosphate (NaH_2PO_4), ethanol, ascorbic acid (AA), uric acid (UA), dopamine (DA) and glucose were purchased from Beijing Chemicals Co., Ltd. (Beijing, China). H_2O_2 (analytical grade, 30% aqueous solution) was supplied by Tianjin Dongfang Chemical Plant (Tianjin, China). The water used was purified through a Millipore system (~18.2 MΩ cm). Carbon-coated Cu grids for transmission electron microscopy (TEM) characterization were purchased from Plano GmbH (Wetzlar, Germany). PU, which was synthesized from dicyclohexylmethylmethane-4,4′-diisocyanate, polycaprolactone glycol and 1,4-butanediol, was kindly provided by the Yantai Wanhua Beijing Research Institute (Beijing, China), and its structure is depicted in Fig. 1, according to the previous report.[37]

2.2 Electrospinning of PU–AgNP, PU–MWCNT and PU–MWCNT–AgNP nanofibers

To uniformly disperse MWCNTs in the PU matrix, MWCNTs were firstly oxidized by heating and refluxing in a mixture of concentrated H_2SO_4 and HNO_3 (3 : 1, v/v) for 24 h. Then AgNPs and the modified MWCNTs were dispersed in HFIP using an ultrasonic cleaner operating at 40 kHz for 30 min, respectively. The resulting dispersions were homogeneous and stable. Meanwhile, PU was dissolved in HFIP to form a uniform transparent solution. Then the dispersions of AgNPs and modified MWCNTs were mixed with PU solutions by stirring, forming four types of spinning solutions (PU, PU–MWCNT, PU–AgNP, and PU–MWCNT–AgNP). The concentrations of PU were

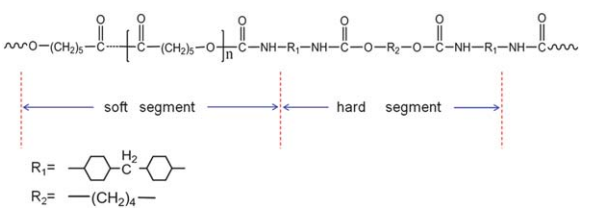

Fig. 1 Structure of PU used in this work.

3 wt% in all the solutions, while the concentrations of MWCNTs in the PU–MWCNT samples were various with 0.5, 1 and 1.5 wt%, and those of AgNPs in the PU–AgNP samples were various with 0.1, 1, 3 and 5 wt%. For the PU–MWCNT–AgNP samples the concentrations of MWCNTs were fixed to be 0.5 wt% and the concentrations of AgNPs varied from 0.1 to 5 wt% as mentioned above. These dispersions were then loaded into plastic 10 mL syringes with an 18 gauge blunt tip needle and were dispensed at a rate of 0.1–0.3 mL h^{-1} during electrospinning. All the samples were electrospun with an applied voltage of 12 kV at a distance of 12 cm from the needle tip to the collector surface of tinfoil.

2.3 Preparation of electrospun nanofiber modified GCE

To prepare the nanofibrous membrane modified GCE, the nanofibers were directly electrospun onto the surface of GCE. The electrospinning setup is schematically shown in Fig. 2, in which the tinfoil and GCE were both connected to the ground. It took two minutes to deposit the nanofibers onto the surface of GCE for each sample. Before electrospinning the GCE was polished with a wet abrasive paper (2000 mesh), then rinsed by sonication in ethanol and water in turn. After electrospinning, the nanofiber modified GCE was dried in a vacuum oven at room temperature for next tests.

2.4 Preparation of Nafion, MWCNT–Nafion, AgNP–Nafion and MWCNT–AgNP–Nafion modified GCEs by the casting method

To demonstrate the highly electrocatalytic performance of our electrospun nanofiber modified electrodes, Nafion, MWCNT–Nafion, AgNP–Nafion and MWCNT–AgNP–Nafion modified GCEs were prepared by traditional casting methods with the use of Nafion solution as control experiments. 4 μL of sample ethanol solutions (MWCNT, AgNP, and MWCNT–AgNP) was dropped onto the surface of pretreated GCEs and then dried in air. After that, 2 μL of Nafion was cast onto the electrodes to avoid the leakage of the materials. The Nafion modified GCE was prepared by directly casting 6 μL of Nafion–ethanol solution (containing 2 μL Nafion) onto the surface of electrode. The concentration ratio of MWCNTs and AgNPs in the MWCNT–AgNP–Nafion modified GCE was 0.5 wt% to 5 wt%; and the amount of Nafion used to modify the GCE in each experiment was the same, maintaining 2 μL. These Nafion, MWCNT–Nafion, AgNP–Nafion and MWCNT–AgNP–Nafion modified GCEs were used for the electrochemical tests.

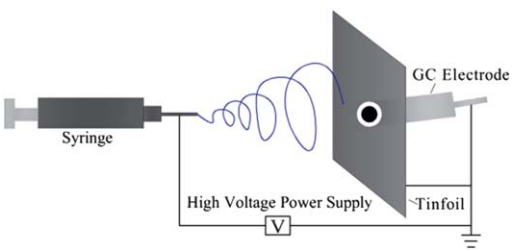

Fig. 2 Schematic of the electrospinning apparatus for preparing the nanofibrous membrane modified GCE.

2.5 Experimental techniques

Morphologies of the electrospun nanofibers were determined through a Hitachi S-4700 scanning electron microscope (SEM, Japan) at 20 kV. TEM images were taken by a JEOL 3010 electron microscope (JEOL Ltd., Tokyo, Japan) at 300 kV coupled with energy dispersive X-ray (EDX) spectroscopy. For the TEM characterization the samples were spun directly on copper grids coated by a holey carbon film.

DSC was conducted on a Mettler-Toledo DSC 822e under a nitrogen atmosphere. The heating rate of the scans was 10 °C min^{-1}, from 20 to 250 °C. DMA was performed on a Perkin-Elmer DMA-7 (Norwalk, CT) at a frequency of 1 Hz. The temperature dependence of the storage modulus and the loss tangent were measured in the temperature range between −80 and 100 °C at a heating rate of 3 °C min^{-1}. Samples with dimensions of 12 × 3 × 0.06 mm^3 were used for the tests.

The conductivity of the nanofiber sheets was measured using an impedance analyzer (Agilent 4294A) over a frequency range of 10^3 to 10^6 Hz. The square nanofiber sheets with an area of 1 cm^2 were sputter-coated by a K-550X sputter coater with Au on both sides before testing.

All electrochemical experiments were performed on a CHI 660A electrochemical workstation (CH Instruments, Shanghai, China) at room temperature. A conventional three-electrode system was employed with a bare or modified GCE as the working electrode, a Pt wire as the auxiliary electrode, and a KCl saturated calomel electrode (SCE) as the reference electrode. The test solutions were phosphate buffer solutions (PBS, 0.1 M) with various pHs, which were prepared with 0.1 M NaH_2PO_4 and 0.1 M Na_2HPO_4 and deoxygenated with highly pure nitrogen for 20 minutes before electrochemical experiments. All potentials in this work refer to the SCE. The curves of cyclic voltammograms (CVs) in this work were obtained after six times of scan numbers under steady-state conditions. Amperometric measurements were carried out under stirred conditions.

3 Results and discussion

3.1 Morphologies of as-spun hybrid nanofibers

To study the morphologies of the as-spun PU–MWCNT–AgNP hybrid nanofibers, SEM and TEM were carried out in this work.

Fig. 3 shows the morphologies of the as-spun PU, PU–MWCNT, PU–AgNP and PU–MWCNT–AgNP nanofibrous membranes, respectively. It can be clearly seen that all the membranes are highly porous, which is beneficial to the diffusion of reactants.[31] The nanofibers of PU and PU–MWCNT are relatively uniform, with smooth surface, and the diameters range from 200 to 400 nm (Fig. 3a and b). While the surface of PU–AgNP nanofibers is much rougher, with many Ag nodules distributed throughout the nanofibers, and the distribution of the nanofiber diameter becomes larger, ranging from about 200 to 800 nm (Fig. 3c). The agglomeration of AgNPs contributed to the Ag nodules distributed throughout the nanofibers.

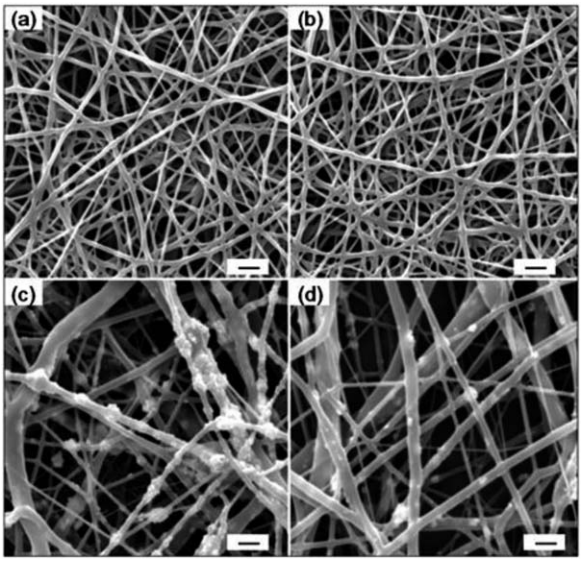

Fig. 3 SEM images of electrospun PU hybrid nanofibers with different nanofillers (MWCNTs or AgNPs): (a) pure PU, (b) PU–MWCNT, (c) PU–AgNP, and (d) PU–MWCNT–AgNP. The scale bar is 2 μm for all pictures.

Interestingly, compared to the PU–AgNP nanofibers, the surface of the electrospun PU–MWCNT–AgNP nanofibers is much smoother and the Ag nodules get less distinct (Fig. 3d), which indicates that the interaction between MWCNTs and AgNPs can facilitate the uniform distribution of AgNPs along the nanofiber matrix.

The distribution of MWCNTs and AgNPs in the PU nanofibrous matrix was further examined by TEM; and the results are shown in Fig. 4. It can be clearly seen that in the PU–AgNP nanofibers, Ag clusters spread throughout the PU matrix discretely, without being connected to each other (Fig. 4a). The inset in Fig. 4a demonstrates the EDX spectrum of the corresponding PU–AgNP hybrid nanofibers. The existence of element Ag can be clearly identified. Fig. 4b and c show that, in both the electrospun PU–MWCNT and PU–MWCNT–AgNP nanofibers, MWCNTs are successfully aligned and oriented in the PU matrix. It should be noted that in the PU–MWCNT–AgNP nanofibers the Ag clusters tend to adhere to the surface of MWCNTs (Fig. 4c), and MWCNTs always act as bridges to combine the discrete Ag clusters together (Fig. 4d). The assembly of MWCNTs and AgNPs can effectively facilitate the electron transfer, thus boosting the conductivity and improving the electrocatalytic performance of the materials.

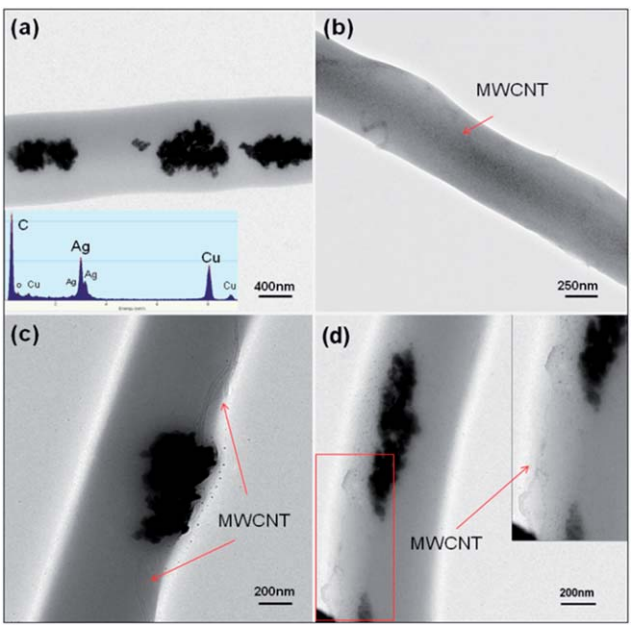

Fig. 4 TEM photographs of (a) PU–AgNP, (b) PU–MWCNT, and (c and d) PU–MWCNT–AgNP hybrid nanofibers. The inset in (a) is the EDX spectrum of PU–AgNP nanofibers, and the inset in (d) is the magnified image of the selected area.

3.2 The interaction between MWCNTs and AgNPs in the PU nanofiber matrix and their influence on the microphase separation structure of the hybrid nanofibers

As SEM and TEM characterizations indicate the binding affinity between AgNPs and MWCNTs in the PU nanofibers, the interaction between them can be examined by thermal analyses. It is well known that the PU molecular chain consists of soft segments (SS) and hard segments (HS) (Fig. 1), and the incompatibility between them induces a microphase separation structure, which can greatly influence the properties of PU, such as thermal properties, crystallization and mechanical behaviours.[37–40]

According to previous reports, both the SS and HS of PU can crystallize independently, and in general the melting temperature of the SS of PU is below 100 °C, while that of the HS of PU is above 100 °C.[37–41] Therefore we examine the first heating DSC traces of the PU and PU hybrid nanofibers embedded with AgNPs and MWCNTs separately or simultaneously (Fig. 5). Fig. 5a shows the effect of the different nanofillers (MWCNTs or AgNPs) on the crystallization of the SS in the electrospun PU nanofibers. It can be clearly seen that the melting point of pure PU nanofibers and PU-MWCNT nanofibers is almost the same, peaking at about 65 °C, which corresponds to the melt of SS.[37,38] While it shifts to about 88 °C for the PU–AgNP nanofibers, indicating that the AgNPs distributed in the SS act as nucleating agents and highly promote the crystallization of SS. However, it is interesting to note that the crystallization behaviour of the SS in the PU–MWCNT–AgNP nanofibers is similar to that in the

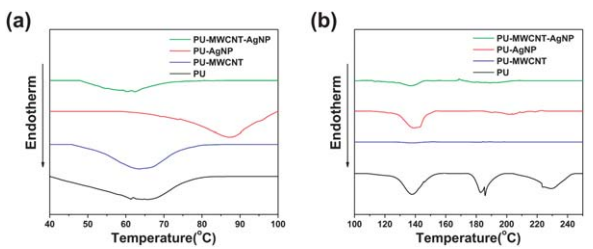

Fig. 5 DSC thermograms of PU and PU hybrid nanofibers filled with AgNPs and MWCNTs separately or simultaneously at the temperature range of (a) 40 to 100 °C and (b) 100 to 250 °C.

PU–MWCNT nanofibers rather than the PU–AgNP ones, which confirms the interaction between MWCNTs and AgNPs in the electrospun nanofibers.

With the continuous heating up, Fig. 5b demonstrates the influence of the incorporation of MWCNTs and AgNPs on the crystallization behaviour of the HS in the PU matrix. For the pure PU nanofibers, three endothermic peaks that are attributed to the melting of the HS appear at about 140, 185 and 230 °C, respectively. HS melting in this temperature range has been reported in a number of previous reports.[37,39–41] For the PU–MWCNT sample, almost no melting peak is observed, demonstrating that MWCNTs nearly destroyed the crystallization of HS of the PU matrix, which indicates the strong interaction between the MWCNTs and the HS of PU nanofibers. For PU–AgNP nanofibers, the melting peak at 140 °C is still preserved, which suggests that the interaction of the HS with the AgNPs is much weaker than that with MWCNTs. However, for PU–MWCNT–AgNP nanofibers, the peak at 140 °C is much smaller than that for PU–AgNP nanofibers, which suggest that the crystallization behaviour of the HS of PU–MWCNT–AgNP nanofibers is similar to that of the PU–MWCNT nanofibers. Combining the results of the analysis for the SS, it can be found that that there exists a clear interaction between AgNPs and the SS of PU, and a significant interaction between MWCNTs and the HS of PU. Therefore, we can deduce that in the electrospun PU hybrid nanofibers AgNPs tend to disperse in the SS, while MWCNTs tend to be present in the HS of the PU matrix.

It should be noted that the crystallization behaviour of the electrospun PU–MWCNT–AgNP nanofibers is similar to that of the PU–MWCNT nanofibers, but vastly different from that of PU–AgNP nanofibers. The simultaneous introduction of MWCNTs and AgNPs into the PU matrix could completely destroy the crystallization of the HS of the PU matrix, but hardly affect the crystallization of the SS. The difference between PU–MWCNT–AgNP and PU–AgNP nanofibers demonstrates the strong interaction between MWCNTs and AgNPs in the PU matrix. Tending to be adhered onto the surface of MWCNTs, as depicted in the TEM figures (Fig. 4), the AgNPs would migrate from the SS of the PU matrix to the HS regions or the interface between them, which explains the crystallization behaviours of the electrospun PU–MWCNT–AgNP nanofibers.

To further investigate the interaction between AgNPs and MWCNTs in the PU matrix and explore the distribution of them in the SS and HS microphase of PU, DMA measurements were carried out according to the previous report.[41] Fig. 6a describes the DMA of tan δ as a function of temperature in the range of −20 to 80 °C. The peak of tan δ coincides with the dynamic glass transition behaviour of the SS of the PU matrix. As shown in Fig. 6a, compared with the pure PU nanofibers the glass transition temperature (T_g) of PU–AgNP nanofibers shows an obvious shift toward higher temperature, while no obvious change of T_g occurs for both the PU–MWCNT and the PU–MWCNT–AgNP nanofibers. These trends can be understood as follows. The T_g is the temperature above which the SS of PU start to become mobile. The results discussed above suggest that the AgNPs physically bonded to the SS and restricted their mobility, leading to an increment of the T_g of PU–AgNP nanofibers. On the other hand, the MWCNTs appear to show only limited interactions with the SS as their presence does not influence T_g. These data reinforce the deduction that the AgNPs tend to highly interact with the SS, whereas the MWCNTs interact preferentially with the HS. Furthermore, unlike the separated addition of AgNPs into the PU matrix, the simultaneous addition of MWCNTs and AgNPs does not show obvious influence on T_g, which further confirms the interaction between AgNPs and MWCNTs in the as-spun PU matrix, and supports the deduction that in the electrospun PU–MWCNT–AgNP nanofibers the AgNPs tend to emigrate from the SS of the PU matrix.

Fig. 6b shows the storage modulus of PU hybrid samples with different nanofillers as a function of temperature. It can be found that all the hybrid samples show a decreased storage modulus compared to the pure PU nanofibers. It is well known that the mechanical properties of PU highly depend on the degree of micro-phase separation: higher degree of micro-phase separation, in general, brings in better mechanical properties.[42] Therefore, the decreases of the storage modulus of the hybrid samples suggest the reduction of the degree of micro-phase separation of the PU matrix. In other words, the addition of MWCNTs and AgNPs could promote the fusion of the SS and HS, and greatly enhance the compatibility of the two microphases.

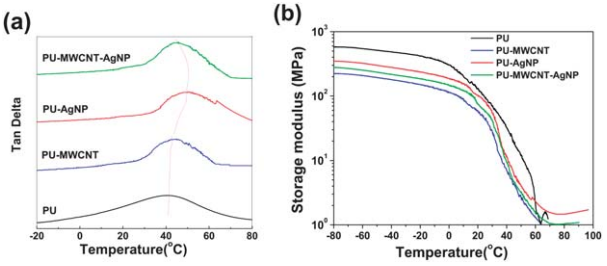

Fig. 6 DMA of (a) tan δ and (b) storage modulus as a function of temperature for PU, PU–MWCNT, PU–AgNP and PU–MWCNT–AgNP nanofibers.

3.3 Electrical properties of electrospun PU–MWCNT–AgNP nanofibers

To evaluate the electrical conductance of PU–MWCNT–AgNP hybrid nanofibers and further explore how the interaction between MWCNTs and AgNPs affects the conductivity of the hybrid nanofibers, impedance analysis was conducted on PU–MWCNT, PU–AgNP and PU–MWCNT–AgNP nanofibers with different concentrations.

Fig. 7 shows the log–log plots of the conductivity and frequency for different PU matrices with different concentrations of MWCNTs and/or AgNPs. The PU–MWCNT nanofiber samples fail to conduct when the concentration of MWCNTs is 1 wt% or lower, but they become conductive when the concentration of MWCNTs is 1.5 wt% (Fig. 7a). The same tendency is found for the PU–AgNP nanofiber samples. They do not show any characteristic of conductivity when the concentration of AgNPs is 3 wt% or lower, but they become conductive

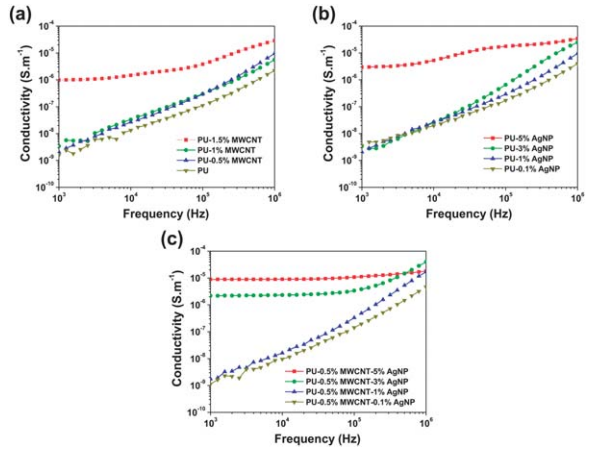

Fig. 7 Log–log plots of the conductivity with respect to frequency for (a) PU–MWCNT nanofibers with different concentrations of MWCNTs, (b) PU–AgNP nanofibers with different concentrations of AgNPs, and (c) PU–MWCNT–AgNP nanofibers with 0.5 wt% MWCNTs and different concentrations of AgNPs.

when the concentration is 5 wt% (Fig. 7b). However, the interesting thing is that when only 0.5 wt% MWCNTs and 3 wt% AgNPs are incorporated into the nanofibers, the PU–MWCNT–AgNP nanofiber samples are conductive (Fig. 7c). In addition, the conductivity of PU–MWCNT–AgNP nanofiber samples can be improved by increasing the concentration of AgNPs. The reduction of the percolation threshold of the PU–MWCNT–AgNP nanofiber mats reveals the synergistic effect of MWCNTs and AgNPs on conductivity. Due to the high aspect ratio of MWCNTs and the orientation effect by electrospinning, only a small amount addition of MWCNTs into the PU–MWCNT–AgNP samples can successfully bridge the discrete AgNP clusters in the as-spun nanofibers, which can effectively facilitate the electron transfer and thus improve the conductivity of the hybrid nanofibers.

Based on the above results, we proposed a model to display the distribution of MWCNTs and AgNPs inside the electrospun nanofibers clearly (Fig. 8). When added separately, the AgNPs agglomerate into clusters and distribute discretely along the nanofibers. They preferentially interact with the SS of PU and are mainly located in the soft phase (Fig. 8a). The MWCNTs incorporated in the electrospun PU nanofibers are highly stretched and oriented along the nanofiber direction, while they preferentially interact with the HS of PU and are mainly located in the hard phase (Fig. 8b). When the AgNPs are incorporated into the PU matrix along with the MWCNTs, they tend to adhere to the surface of MWCNTs that mainly dispersed in the hard phase, and show limited interaction with the SS (Fig. 8c). The aligned MWCNTs act as bridges and get the discrete Ag clusters in series, which results in a notable synergistic effect and endows the PU–MWCNT–AgNP nanofibers with good conductivity and great potential in the application of electrochemical sensors.

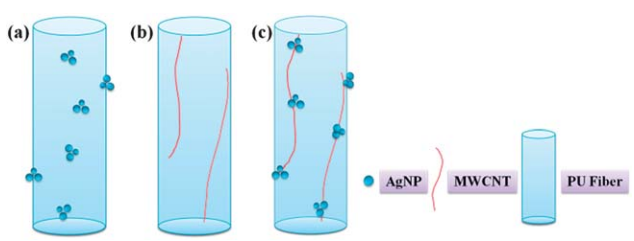

Fig. 8 A proposed model for the dispersion of AgNPs or/and MWCNTs in (a) PU–AgNP, (b) PU–MWCNT and (c) PU–MWCNT–AgNP nanofibers, respectively.

3.4 Potential application in sensing of H_2O_2

3.4.1 Electrocatalytic behaviour of the hybrid nanofiber modified GCE towards H_2O_2. Considering the good electrocatalytic performance of AgNPs and the excellent conductivity of PU–MWCNT–AgNP nanofibers, the prepared PU–MWCNT–AgNP hybrid nanofibers are expected to have better performance than either PU–MWCNT or PU–AgNP nanofibers for the fabrication of electrochemical sensors. To test this hypothesis, PU–MWCNT–AgNP nanofibers were directly electrospun onto the surface of a polished GCE, and the performance of the nanofiber modified GCE for H_2O_2 sensing was investigated in this work. To discern the contribution of individual components and the possible synergistic effect among them, control experiments on electrospun nanofibers with pure PU, PU–MWCNT, and PU–AgNP nanofiber modified GCEs were also carried out.

Fig. 9a shows the CVs of electrospun PU, PU–MWCNT, PU–AgNP and PU–MWCNT–AgNP nanofiber modified GCEs in the presence of 10 mM H_2O_2 at a scan rate of 50 mV s^{-1}. The concentration of MWCNTs and/or AgNPs in the electrospun nanofibers is fixed at 0.5 wt% and 5 wt%, respectively. As can be seen in Fig. 9a, a pure electrospun PU nanofiber modified GCE shows no apparent redox processes. After modified with electrospun PU–MWCNT nanofibers, the diffused current increased clearly, because MWCNTs have a catalytically active surface, and therefore they can increase the active surface area of the modified electrode.[4] Similar to the pure PU nanofiber modified GCE, no obvious redox current peaks appear in the CV of PU–MWCNT nanofiber modified GCE either. For the PU–AgNP nanofiber modified GCE, a large current response and a broad reduction peak from about −0.65 to −0.4 V is observed due to the reduction of H_2O_2. Notably, in the CV of PU–MWCNT–AgNP nanofiber modified GCE, the reduction peak occurs at

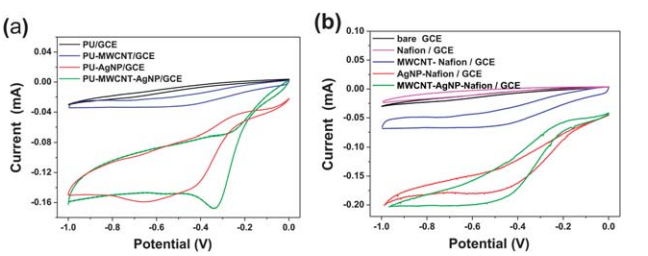

Fig. 9 CVs of electrospun (a) PU, PU–MWCNT, PU–AgNP, and PU–MWCNT–AgNP nanofiber modified GCEs, and (b) bare GCE and GCEs modified with Nafion, MWCNT–Nafion, AgNP–Nafion and MWCNT–AgNP–Nafion separately by a casting method. All the tests were performed in 0.1 M N_2 saturated PBS (pH 7.6) and in the presence of 10 mM H_2O_2 at a scan rate of 50 mV s^{-1}.

about −0.34 V, and there is an obvious positive shift of both the onset potential and current peak as compared to that of the PU–AgNP nanofiber modified GCE. The present CV results indicate that the PU–MWCNT–AgNP nanofiber modified GCE has better electrocatalytic activity than either PU–MWCNT nanofibers or PU–AgNP nanofiber modified GCE toward the reduction of H_2O_2, which confirms the synergistic effect of MWCNTs and AgNPs.

To prove the advantage of the electrospun nanofibers in electrochemical sensing, suspension of Nafion, MWCNT–Nafion, AgNP–Nafion and MWCNT–AgNP–Nafion were directly cast onto the surfaces of polished GCEs separately, fabricating Nafion, MWCNT–Nafion, AgNP–Nafion and MWCNT–AgNP–Nafion modified GCEs, respectively, as control experiments. The CV results of these electrodes are depicted in Fig. 9b. It can be found that neither bare GCE nor Nafion modified GCE shows a characteristic peak in response to H_2O_2 and the MWCNT–Nafion modified GCE has no obvious redox peak either. A board peak at a potential of about −0.4 V is observed for the AgNP–Nafion modified GCE due to the reduction of H_2O_2. Unlike the remarkable improvement of electrocatalytic activity observed in the PU–MWCNT–AgNP electrospun nanofiber modified GCE, no substantial difference of the electrochemical activity is observed between GCEs modified with AgNP–Nafion and MWCNT–AgNP–Nafion by a casting method.

Comparing the results shown in Fig. 9a and b, it can be clearly found that the onset potential for H_2O_2 reduction in the PU–MWCNT–AgNP nanofiber modified electrode appears more positive than its counterpart electrode modified by a casting method, which reveals the superiority of the electrospun nanofibers in electrochemical sensing of H_2O_2. We suggest that the superiority is ascribed to the advantages of the electrospinning technique. Firstly, during the electrospinning process, MWCNTs can be successfully dispersed and aligned along the nanofiber direction. Since in the presence of MWCNTs the AgNPs tend to adhere onto their surface, the well dispersion and orientation of MWCNTs in the electrospun nanofibers can facilitate the dispersion of AgNPs along the nanofibers (Fig. 3), which can effectively increase the active surface of the modified electrodes and improve the electrocatalytic activity of electrodes. Secondly, according to our previous study the orientation of MWCNTs in the nanofiber matrix can facilitate the formation of a conductive path throughout the materials,[43] which is in favor of the electron transfer during the redox reaction and can increase the diffusion current. Thirdly, the electrospun membranes are highly porous, as can be seen from the SEM photographs (Fig. 3). This porous structure can greatly increase the effective electrode area and facilitate the adsorption of electrolytes and the diffusion of reactants, which can further help enhancing the electrocatalytic activity of electrodes.[31]

3.4.2 Optimization of experimental variables. The effect of the pH of the buffer solution on the biosensor response was studied between 5.7 and 8.6 in 0.1 M PBS in the presence of 1 mM H_2O_2. Fig. 10 shows the amperometric responses of MWCNT–AgNP–Nafion, PU–MWCNT–AgNP nanofibers and PU–AgNP nanofiber modified GCE, respectively. For the MWCNT–AgNP–Nafion modified GCE, the current value is in general higher than that of the nanofiber modified electrodes. It is because the current value highly relies on the amount of AgNPs, and there were a larger amount of AgNPs on the surface of the MWCNT–AgNP–Nafion modified GCE than that of the GCEs modified by electrospun nanofibers, considering the fact that it just took about two minutes to fabricate an electrospun nanofiber modified GCE. In addition, the current value of the PU–MWCNT–AgNP modified GCE is generally higher when compared with that of the PU–AgNP modified GCE, which is due to the remarkable synergistic effect of MWCNTs and AgNPs. Moreover, the influence of pH on the biosensor responses of the three kinds of electrodes is clearly demonstrated in Fig. 10. The trend is as follows. Firstly, the steady-state current sharply increased with the increasing pH value and arrived at a maximum at the pH value of 7.6. Then the current declined as pH increased. Therefore, in order to get a sensitive response, the PBS at pH 7.6 was selected for the next experiments.

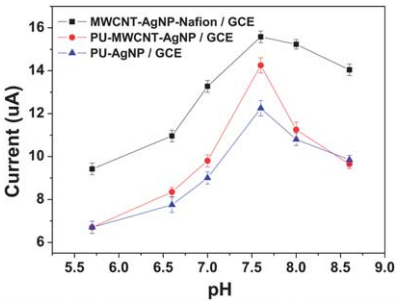

Fig. 10 Effect of pH on the amperometric steady-current responses of MWCNT–AgNP–Nafion, PU–MWCNT–AgNP nanofibers and PU–AgNP nanofiber modified GCE, respectively. All the tests were performed in the presence of 1 mM H_2O_2 and 0.1 M PBS with an applied potential of −0.34 V *vs.* SCE.

3.4.3 Chronoamperometric response and calibration curve. To check the electrocatalytic performance of electrospun PU–MWCNT–AgNP nanofibers toward H_2O_2 and further identify the synergistic effect between MWCNTs and AgNPs in the electrospun nanofibers, the chronoamperometry of the electrodes modified with electrospun PU–AgNP and PU–MWCNT–AgNP nanofibers was performed at an applied potential of −0.34 V *vs.* SCE. As is shown in Fig. 11, both modified electrodes show stable response over the long test period and rapid increase in the cathodic current as a result of the reduction of H_2O_2 upon the addition of H_2O_2 solution. However, the response currents of the PU–MWCNT–AgNP nanofiber modfied electrode (Fig. 11b) are much larger than that modified with PU–AgNP nanofibers (Fig. 11a). This improvement can be ascribed to the synergistic amplification effect of MWCNTs and AgNPs in the electrospun nanofibers. The insets in Fig. 11 are amplifications of the current–time curves obtained with lower H_2O_2 inject concentrations, and the results show that the limit of detection (LOD) of the PU–MWCNT–AgNP nanofiber modified GCE is lower than that of the GCE modified with the PU–AgNP nanofibers.

The advantage of PU–MWCNT–AgNP nanofibers based electrochemical biosensors for detecting H_2O_2 over that based on PU–AgNP nanofibers is clearly demonstrated through the calibration curves. Fig. 12 shows the steady-state calibration

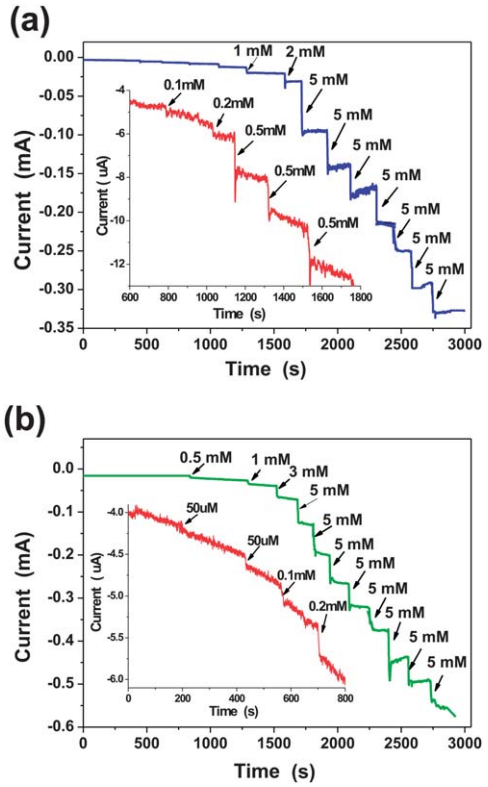

Fig. 11 Current–time response of (a) PU–AgNP and (b) PU–MWCNT–AgNP nanofiber modified GCE in 0.1 M pH 7.6 PBS with successive addition of H_2O_2 at −0.34 V *vs.* SCE. (The insets are the current–time curves obtained at the PU–AgNP nanofiber modified GCE upon increasing the concentration of H_2O_2 in steps of 0.1, 0.2 and 0.5 mM, and that obtained at the PU–MWCNT–AgNP nanofiber modified GCE upon increasing the concentration of H_2O_2 in steps of 0.05, 0.1 and 0.2 mM.)

curves of the PU–AgNP and PU–MWCNT–AgNP nanofiber modified GCEs. The experimental results indicate that both electrodes reveal a linear response to H_2O_2. For the PU–AgNP nanofiber modified electrode, the linear range of the H_2O_2 detection is from 1 to 25 mM (R = 0.9998), and the LOD is calculated to be 36.3 μM ($S/N = 3$) with a sensitivity of 117.5 μA mM^{-1} cm^{-2}. While for the PU–MWCNT–AgNP nanofibers modified electrode, the biosensor has a linear detection range from 0.5 to 30 mM ($R = 0.9999$), and possesses a LOD of 18.6 μM ($S/N = 3$) with a sensitivity of 160.6 μA mM^{-1} cm^{-2}. Based on the above results, we believe that the electrospun PU–MWCNT–AgNP nanofiber modified electrode shows improved performances for sensing H_2O_2 compared to the PU–AgNP nanofiber modified electrode, and this improvement can be attributed to the large catalytically electroactive surface area of the fabricated electrode materials, the better dispersion of AgNPs, and the synergistic amplification effect of MWCNTs and AgNPs.

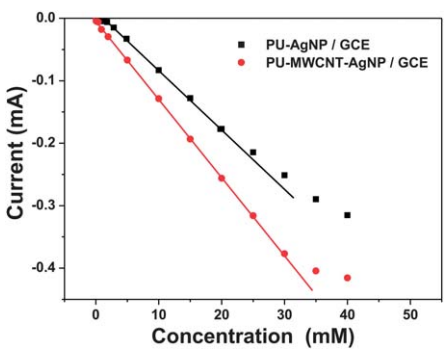

Fig. 12 Calibration curve of PU–MWCNT–AgNP and PU–AgNP nanofiber modified GCEs at −0.34 V *vs.* SCE in the H_2O_2 concentration range of 0.05–40 mM.

3.4.4 Selectivity, reproducibility and stability. The selectivity and anti-interference capability of the PU–MWCNT–AgNP modified GCE were evaluated by amperometry in the presence of AA, UA, DA and glucose, which are common interfering substances for the detection of H_2O_2.[44] Fig. 13a presents the amperometric responses of the PU–MWCNT–AgNP modified GCE for the successive addition of 1 mM of H_2O_2, 0.1 mM of AA,

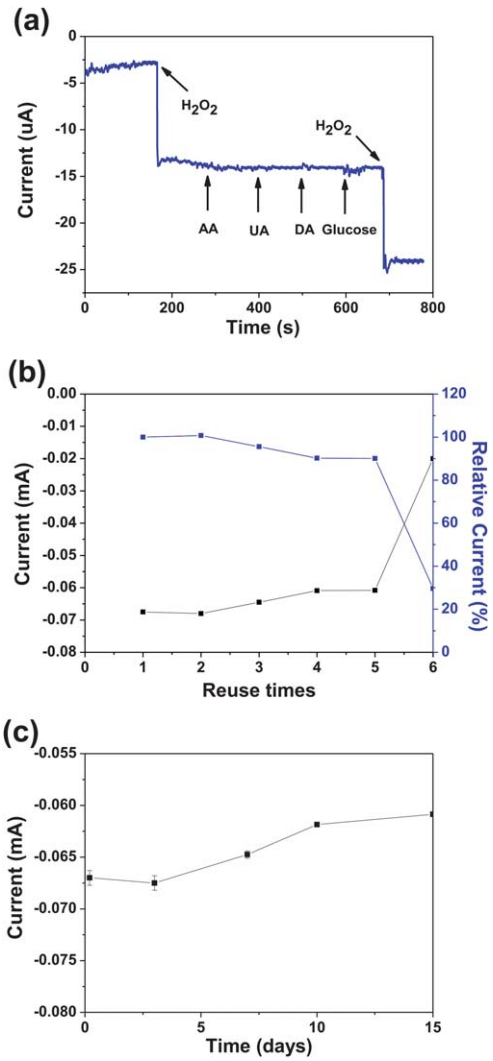

Fig. 13 Typical steady-state response of the PU–MWCNT–AgNP modified GCE in N_2 saturated PBS (0.1 M, pH 7.6) at an applied potential of −0.34 V *vs.* SCE. (a) Amperometric responses upon successive addition of 1 mM of H_2O_2, 0.10 mM of AA, 0.10 mM of UA, 0.10 mM of DA, 5.0 mM of glucose, and 1 mM of H_2O_2, (b) reusability and (c) the long-term storage stability in the response to 5 mM H_2O_2.

0.10 mM of UA, 0.10 mM of DA, 5.0 mM of glucose and 1 mM of H_2O_2. It can be seen that the interferences which these species may have on H_2O_2 detection are negligible, suggesting a high selectivity of the biosensor based on the PU–MWCNT–AgNP modified GCE.

The reuse stability of the PU–MWCNT–AgNP modified GCE was also assessed in Fig. 13b, showing that at least 5 times of use of the created biosensor is possible. Significant reduction in current after 5 times of use is depicted (Fig. 13b), which was ascribed to the detachment of the membrane from the electrode.[27] Therefore, reinforcement of the interfacial adhesion between the nanofibrous membrane and the electrode for further improving the reusability will be necessary in the future work.

The long-term stability of the PU–MWCNT–AgNP modified GCE was explored over a 15-day period (Fig. 13c). The fabricated sensor was stored in the refrigerator at 4 °C and measured every 3–5 days. The result shows that the catalytic current response maintains more than 90.2% of its initial value in response to 5 mM H_2O_2 after 15 days, indicating an acceptable stability of the modified electrode.

4 Conclusions

In summary, we demonstrated a facile and effective strategy to prepare a new non-enzymatic H_2O_2 biosensor based on electrospun PU–MWCNT–AgNP hybrid nanofibers on a chemical electrode. The synergistic effect of MWCNTs and AgNPs can significantly improve the conductivity of electrospun nanofibers, and the electrocatalytic activity and sensitivity of this non-enzymatic biosensor. The electrochemical results proved that the electrospun PU–MWCNT–AgNP nanofiber modified GCEs reveal better electrocatalytic activity toward H_2O_2 than the electrodes modified by traditional casting strategy. The LOD of this electrospun PU–MWCNT–AgNP nanofiber based biosensor for H_2O_2 is about 18.6 μM ($S/N = 3$) with high sensitivity. By introducing different functional nanomaterials and building blocks into the polymer nanofibers, this electrospinning technique will be very helpful for fabricating other kinds of sensors with high performance.

Acknowledgements

We acknowledge the financial support from the National Natural Science Foundation of China (Grant no. 20974010) and Beijing New-Star Program of Science and Technology (Grant no. 2009B10). We would like to thank the financial support from the German Academic Exchange Council (DAAD) for a short-term scholarship and the China Scholarship Council (CSC) for a PhD scholarship.

Notes and references

1 M. Somasundrum, K. Kirtikara and M. Tanticharoen, *Anal. Chim. Acta*, 1996, **319**, 59.
2 P. N. Bartlett, P. R. Birkin, J. H. Wang, F. Palmisano and G. D. Benedetto, *Anal. Chem.*, 1998, **70**, 3685.
3 M. Darder, K. Takada, F. Pariente, E. Lorenzo and H. D. Abruna, *Anal. Chem.*, 1999, **71**, 5530.
4 W. Zhao, H. Wang, X. Qin, X. Wang, Z. Zhao, Z. Miao, L. Chen, M. Shan, Y. Fang and Q. Chen, *Talanta*, 2009, **80**, 1029.
5 C. Matsubara, N. Kawamoto and K. Takamura, *Analyst*, 1992, **117**, 1781.
6 X. Li, G. Zhang, H. Ma, D. Zhang, J. Li and D. Zhu, *J. Am. Chem. Soc.*, 2004, **126**, 11543.
7 M. W. Shao, Y. Y. Shan, N. B. Wong and S. T. Lee, *Adv. Funct. Mater.*, 2005, **15**, 1478.
8 M. Y. Hua, H. C. Chen, C. K. Chuang, R. Y. Tsai, J. L. Jeng, H. W. Yang and Y. T. Chern, *Biomaterials*, 2011, **32**, 4885.
9 S. Park, H. Boo and T. D. Chung, *Anal. Chim. Acta*, 2006, **556**, 46.
10 Y. Ye, T. Kong, X. Yu, Y. Wu, K. Zhang and X. Wang, *Talanta*, 2012, **89**, 417.
11 C. M. Welch, C. E. Banks, A. O. Simm and R. G. Compton, *Anal. Bioanal. Chem.*, 2005, **382**, 12.
12 Y. Song, K. Cui, L. Wang and S. Chen, *Nanotechnology*, 2009, **20**, 105501.
13 J. Xuan, X. D. Jia, L. P. Jiang, E. S. Abdel-Halim and J. J. Zhu, *Bioelectrochemistry*, 2012, **84**, 32.
14 A. Wang, X. Ye, P. He and Y. Fang, *Electroanalysis*, 2007, **19**, 1603.
15 M. R. Guascito, E. Filippo, C. Malitesta, D. Manno, A. Serra and A. Turco, *Biosens. Bioelectron.*, 2008, **24**, 1057.
16 W. Li, C. Liang, J. Qiu, W. Zhou, H. Han, Z. Wei, G. Sun and Q. Xin, *Carbon*, 2002, **40**, 787.
17 N. Rajalakshmi, H. Ryu, M. M. Shaijumon and S. Ramaprabhu, *J. Power Sources*, 2005, **140**, 250.
18 Y. Shi, Z. Liu, B. Zhao, Y. Sun, F. Xu, Y. Zhang, Z. Wen, H. Yang and Z. Li, *J. Electroanal. Chem.*, 2011, **656**, 29.
19 S. Hrapovic, Y. Liu, K. B. Male and J. H. T. Luong, *Anal. Chem.*, 2004, **76**, 1083.
20 M. N. Bui, X. Pham, K. N. Han, C. A. Li, Y. S. Kim and G. H. Seong, *Sens. Actuators, B*, 2010, **150**, 436.
21 P. Norouzi, B. Larijani, F. Faridbod and M. R. Ganjali, *Int. J. Electrochem. Sci.*, 2010, **5**, 1550.
22 G. G. Wildgoose, C. E. Banks, H. C. Leventis and R. G. Compton, *Microchim. Acta*, 2006, **152**, 187.
23 G. W. Yang, G. Y. Gao, C. Wang, C. L. Xu and H. L. Li, *Carbon*, 2008, **46**, 747.
24 W. T. Wu, L. Shi, Y. Wang, W. Pang and Q. Zhu, *Nanotechnology*, 2008, **19**, 125607.
25 G. Wei, F. Xu, Z. Li and K. D. Jandt, *J. Phys. Chem. C*, 2011, **115**, 11453.
26 W. E. Teo and S. Ramakrishna, *Compos. Sci. Technol.*, 2009, **69**, 1804.
27 Z. G. Wang, Y. Wang, H. Xu, G. Li and Z. K. Xu, *J. Phys. Chem. C*, 2009, **113**, 2955.
28 G. Ren, X. Xu, Q. Liu, J. Cheng, X. Yuan, L. Wu and Y. Wan, *React. Funct. Polym.*, 2006, **66**, 1559.
29 K. Sawicka, P. Gouma and S. Simon, *Sens. Actuators, B*, 2005, **108**, 585.
30 Z. G. Wang, B. B. Ke and Z. K. Xu, *Biotechnol. Bioeng.*, 2007, **97**, 708.

31 Y. Liu, J. Huang, H. Hou and T. You, *Electrochem. Commun.*, 2008, **10**, 1431.
32 J. Huang, D. Wang, H. Hou and T. You, *Adv. Funct. Mater.*, 2008, **18**, 441.
33 B. Wang, L. Luo, Y. Ding, D. Zhao and Q. Zhang, *Colloids Surf., B*, 2012, **97**, 51.
34 R. Liu, S. Li, X. Yu, G. Zhang, Y. Ma and J. Yao, *J. Mater. Chem.*, 2011, **21**, 14917.
35 N. J. Amoroso, A. D'Amore, Y. Hong, W. R. Wagner and M. S. Sacks, *Adv. Mater.*, 2011, **23**, 106.
36 N. Wang, K. Burugapalli, W. Song, J. Halls, F. Moussy, A. Ray and Y. Zheng, *Biomaterials*, 2013, **34**, 888.
37 L. May-Hernández, F. Hernández-Sánchez, J. L. Gomez-Ribelles and R. S. Serra, *J. Appl. Polym. Sci.*, 2011, **119**, 2093.
38 B. Bogdanov, V. Toncheva, E. Schacht, L. Finelli, B. Sarti and M. Scandola, *Polymer*, 1999, **40**, 3171.
39 K. Kojio, S. Nakashima and M. Furukawa, *Polymer*, 2007, **48**, 997.
40 T. K. Chen, T. S. Shieh and J. Y. Chui, *Macromolecules*, 1998, **31**, 1312.
41 U. Khan, F. M. Blighe and J. N. Coleman, *J. Phys. Chem. C*, 2010, **114**, 11401.
42 C. S. Paik Sung, T. W. Smith and N. H. Sung, *Macromolecules*, 1980, **13**, 117.
43 Z. Su, J. Li, Q. Li, T. Ni and G. Wei, *Carbon*, 2012, **50**, 5605.
44 X. Bian, K. Guo, L. Liao, J. Xiao, J. Kong, C. Ji and B. Liu, *Talanta*, 2012, **99**, 256.